Vietnam Journal of Earth Sciences, 44(3), 395-409, https://doi.org/10.15625/2615-9783/17013

Vietnam Academy of Science and Technology
Vietnam Journal of Earth Sciences
http://www.vjs.ac.vn/index.php/jse

Determination of subsurface lineaments in the Hoang Sa islands using enhanced methods of gravity total horizontal gradient

Luan Thanh Pham[1*], Erdinc Oksum[2], Ozkan Kafadar[3], Phan Trong Trinh[4,5], Dat Viet Nguyen[1], Quynh Thanh Vo[1], Sang Thi Le[1], Thanh Duc Do[1]

[1]*University of Science, Vietnam National University, Hanoi, Vietnam*
[2]*Department of Geophysical Engineering, Engineering Faculty, Süleyman Demirel University, Isparta, Turkey*
[3]*Department of Computer Technologies, Kocaeli University, Kocaeli, Turkey*
[4]*Institute of Geological Sciences, VAST, Hanoi, Vietnam*
[5]*Royal Academy for Overseas Sciences, Brussels, Belgium*

Received 08 November 2021; Received in revised form 05 February 2022; Accepted 16 April 2022

ABSTRACT

The Hoang Sa islands, located in the northern part of the East Vietnam Sea, lack information on geological structural boundaries. The gravity data from the global marine gravity model were analyzed using the enhanced total horizontal gradient methods to delineate geological structures that appear as lineaments on the transformed gravity anomaly maps of the area. Before applying the techniques to gravity data of the Hoang Sa islands, their effectiveness was demonstrated by comparing them with the results from the total horizontal gradient method for a synthetic model. Applying the enhanced horizontal gradient methods shows that most of the lineaments identified in the Hoang Sa islands are trending in the WSW-ENE, NE-SW, E-W, WNW-ESE and NNW-SSE directions. These results provide a better understanding of the subsurface structural features of the islands.

Keywords: Gravity, enhanced total horizontal gradient methods, Hoang Sa islands.

1. Introduction

One of the classic applications of the potential field methods is to depict lineaments in potential field data using various filtering techniques (Saibi et al., 2008; Kafadar 2017; Eldosouky et al., 2021a, b; Echogdali et al., 2021). This process is important since the detected lineaments generally correspond to the lateral boundaries of the geological structures (Oksum et al., 2019, 2021a). Many edge detection and enhancement techniques are developed for interpreting potential field data in the literature (Eldosouky et al., 2020; Pham 2020; Pham et al., 2021a, b). The total horizontal gradient method (THG) is a conventional detector commonly used for edge estimation (Cordell and Grauch, 1985). The analytic signal is another popular technique used to detect the boundaries of subsurface structures (Roest et al., 1992). Although these conventional techniques are prevalent methods used to interpret potential field data, they can produce false information

*Corresponding author, Email: luanpt@hus.edu.vn

or bring images in low resolution (Prasad et al., 2022; Eldosouky et al., 2022a, b, c; Ghomsi et al., 2022a). To overcome the limitations of these traditional techniques, researchers have proposed several other approaches based on the gradients of potential fields. For instance, Miller and Singh (1994) introduced the tilt derivative technique based on the arctan function of the ratio of the vertical gradient to the THG. Fedi and Florio (2001) introduced an enhancement of the THG calculated by taking the gradient of a sum of the vertical gradients. Verduzco et al. (2004) suggested a detector based on the gradient amplitude of the tilt derivative. Wijns et al. (2005) proposed the theta technique that normalizes the total gradient using the gradient amplitude. Cooper and Cowan (2006) introduced the normalized gradient amplitude technique. Tatchum et al. (2011) developed a technique (THGVD) based on the gradient amplitude of the vertical gradient. Ferreira et al. (2013) presented the BTHG method known as the tilt angle of the THG. Pham et al. (2020a, 2021c) presented an enhanced version of the horizontal gradient amplitude (EHGA), and softsign function (SF) filters that are based on the derivatives of the THG. Apart from the techniques mentioned above, many other methods in the literature also rely on potential field data gradients. (Hsu et al., 1996; Cooper and Cowan, 2008; Beiki, 2010; Kha et al., 2018; Pham et al., 2018b, 2020a, b; 2021c; Nasuti et al., 2019; Oksum et al., 2021b; Melouah and Pham, 2021; Pham 2021; Kafadar, 2022).

The Hoang Sa islands (Paracel islands) is formed in the formation and evolution process of the East Vietnam Sea (Guo et al., 2016). The study area is located among the South China block, Indochina block, and central basin of the East Vietnam Sea between 109.5°E to 114°E and between 15°N and 18°N (Fig. 1a). There are many gases and oil-bearing Cenozoic sedimentary basins around the Hoang Sa islands (Guo et al., 2016). These basins provide a favorable environment for forming and accumulating petroleum (Guo et al., 2016). Thus, the knowledge of the geological structures of the Hoang Sa islands has an essential role in providing significant guidance for exploring these hydrocarbon basins. There are many studies based on interpreting gravity data for describing geological structures of the East Vietnam Sea. Dung TT et al. (2013) and Trung and Huong (2013) applied the Blakely and Simpson's algorithm to the total horizontal gradient of gravity data to determine the fault systems of the East Vietnam Sea. Since their calculations cover a very large area, their estimated structure images in the Hoang Sa islands are of low resolution. In addition, their studies are based on gravity data from a previous global marine gravity model (Version 18.1) that is less accurate than the current model (Version 29.1) (Sandwell et al., 2014). Dung NK et al. (2019) used the curvature gravity gradient tensor to estimate density boundaries in the Hoang Sa and Truong Sa islands. Although their structure maps have high resolution, the obtained boundaries are connected, complicating the geological interpretation. Inversion of gravity data is a different type of processing, has been performed by many authors in the East Vietnam Sea area (Trung and Huong, 2013; Long et al., 2021). Braitenberg et al. (2006) estimated the depth to the basement from the satellite gravity data. Trung and Huong (2013) and Bai et al. (2014) applied the Parker-Oldenburg method to the satellite gravity data for determining the Moho depth. Dung T.T. et al. (2019) used the satellite and shipboard gravity data to detect the Cenozoic structures in the East Vietnam Sea. Li et al. (2019) used the satellite data for determining the Moho depth of the Hoang Sa islands. Previous gravity studies were concentrated on computing the depths of density interfaces or covered a very large area; therefore, it lacks detailed information about the boundaries of geological structures in the islands.

In this study, the enhanced total horizontal gradient methods have been applied to the gravity data from the high-resolution global marine gravity model (Sandwell et al., 2014) to determine the geological features of the Hoang Sa islands. The effectiveness methods have been estimated on a density model before applying to real data of the study area.

2. Geological setting

The East Vietnam Sea formed by seafloor spreading is a marginal sea of the Western Pacific (Tapponnier et al., 1986; Liem et al., 2021). It is situated at the intersection of the Australian, Eurasian and Indian plates (Luong et al., 2021). The East Vietnam Sea is bounded to the west by the Indochina Peninsula, to the east by the Manila trench, to the south by Borneo, and the north by the shores of South China. The oceanic crust age of the East Vietnam Sea has been dated to be Paleogene to Middle Miocene (Briais et al., 1993), which rests mainly on interpreting the marine magnetic anomaly (Taylor and Hayes, 1983). Based on structural variations, the East Vietnam Sea can be divided into sub-basins such as the Southwest, Northwest, and East subbasins (Pham et al., 2021e).

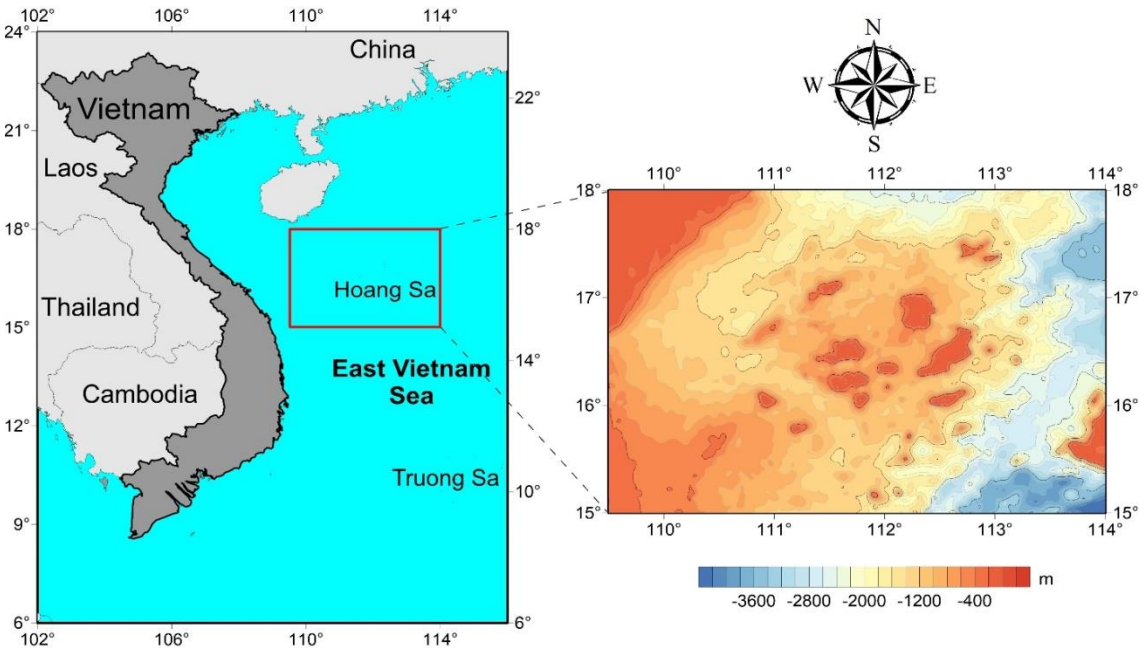

Figure 1. (a) Location of the Hoang Sa islands area, (b) Bathymetry map

The Hoang Sa islands is located in the northern region of the East Vietnam Sea (Fig. 1a). The study area consists of a series of islands, shoals, and reefs. Fig. 1b shows the bathymetry map of the place where the ocean floor depth is in the range of a few tens of meters up to 4000 m (Smith and Sandwell, 1997). Fig. 2a shows the tectonic map of the area with the appearance of the Hoang Sa uplift in the central region (Lu et al., 2018). The Hoang Sa islands and its adjacent areas were affected by rifting and seafloor spreading at the northern margin of the East Vietnam Sea (Tapponnier et al., 1986; Briais et al., 1993). The continental rifting occurred between the Eocene and Paleocene in the southern South China block, and the Hoang Sa uplift was separated from the mainland by the subduction of the East Vietnam Sea oceanic crust (Wu et al., 2021). Then, the sea floor began to spread in the Northwest subbasin during the Oligocene. During this

spreading, the Hoang Sa uplift moved southward away from the South China craton and was submerged in the water (Wu et al., 2021). The submersion of the Hoang Sa uplift provides suitable conditions for carbonate factory development (Wu et al., 2021).

3. Data

The Free-air gravity dataset of the Hoang Sa islands was generated from the global marine gravity model (Sandwell et al., 2014) (Fig. 2b). It is a global gravity field model (Version 29.1) with high resolution, which contains data from CryoSat-2 and Jason-1 satellites (Sandwell et al., 2014). The gravity data from this model have much lower errors than those from the previous gravity model (Sandwell et al., 2014). The 1'×1' free-air anomaly data from the model were used to calculate the Bouguer gravity data of the Hoang Sa islands (Fig. 5a) with a seawater density of 1.03 g/cm^3 and a crust density of 2.67 g/cm^3 (Ghomsi et al., 2022b). The Bouguer gravity data range from 13 mGal to 254 mGal, with high amplitude signals appearing in the eastern region of the area (Fig. 5a). In recent years, the use of gravity data from the global marine gravity model in detecting geological structures has shown great success (Kha and Trung, 2020; Trung et al., 2018, 2020; Pham et al., 2021d, e; Oksum et al., 2021b; Ghomsi et al., 2022b; Tang et al., 2022, Yu et al., 2022).

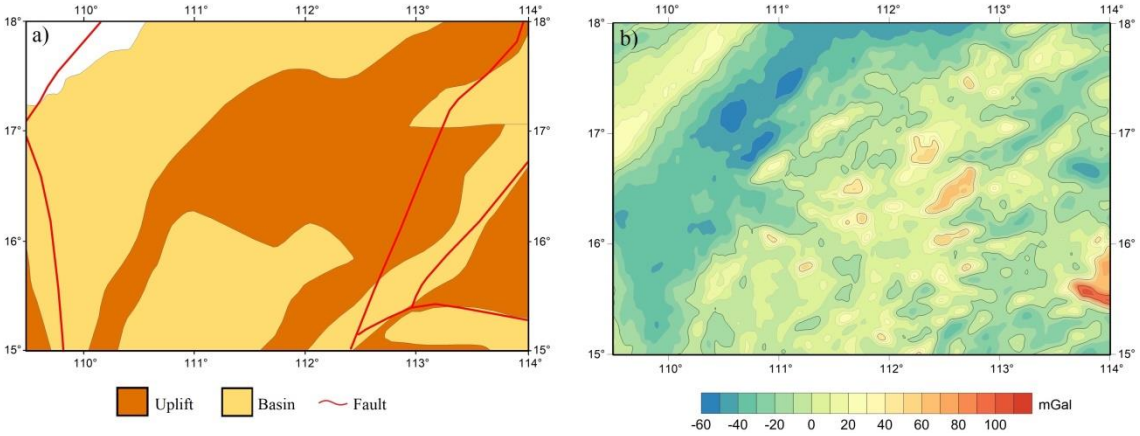

Figure 2. (a) Tectonic map (modifed from Lu et al., 2018) with the faults shown by red lines (Xu et al., 2014), (b) Free-Air gravity data of the Hoang Sa islands area

4. Methods

The THG is one of the most commonly used detectors for enhancement of the borders of the geology structures. The THG of the field F is expressed as follows (Cordell and Grauch, 1985):

$$THG = \sqrt{\left(\frac{\partial F}{\partial x}\right)^2 + \left(\frac{\partial F}{\partial y}\right)^2}. \qquad (1)$$

The THG is less effective when the anomalous bodies are interfered by nearby sources (Fedi and Florio, 2001). Tatchum et al. (2011) proposed the THGVD method to improve the performance of the THG method:

$$THGVD = \sqrt{\left(\frac{\partial VD}{\partial x}\right)^2 + \left(\frac{\partial VD}{\partial y}\right)^2}, \qquad (2)$$

where VD is the vertical gradient of magnetic or gravity data.

The BTHG detector claims to be able to simultaneously bring the border of shallow and deep structures. This detector is formulated as follows (Ferreira et al., 2013):

$$BTHG = atan\left(\frac{\frac{\partial THG}{\partial z}}{\sqrt{\left(\frac{\partial THG}{\partial x}\right)^2 + \left(\frac{\partial THG}{\partial y}\right)^2}}\right). \quad (3)$$

The EHGA method is another technique that can overcome the balance problem encountered in the edge detection studies and uses the following equation (Pham et al., 2020a):

$$EHGA = \mathcal{R}\left(asin\left(p\left(\frac{\frac{\partial THG}{\partial z}}{\sqrt{\left(\frac{\partial THG}{\partial x}\right)^2 + \left(\frac{\partial THG}{\partial y}\right)^2 + \left(\frac{\partial THG}{\partial z}\right)^2}} - 1\right) + 1\right)\right), \quad (4)$$

where p is a constant. Pham et al. (2020a) showed that the best results can be obtained by using p values of 2 or greater.

Another filter for enhancement of the edges is introduced by Pham et al. (2021c) which is based on the softsign function and the derivatives of the THG. The filter is given by:

$$SF = \frac{k \times \frac{\partial THG}{\partial z} - (k+2)\sqrt{\left(\frac{\partial THG}{\partial x}\right)^2 + \left(\frac{\partial THG}{\partial y}\right)^2}}{\sqrt{\left(\frac{\partial THG}{\partial x}\right)^2 + \left(\frac{\partial THG}{\partial y}\right)^2} + \left|k \times \frac{\partial THG}{\partial z} - (k+1)\sqrt{\left(\frac{\partial THG}{\partial x}\right)^2 + \left(\frac{\partial THG}{\partial y}\right)^2}\right|}, \quad (5)$$

where *k* is decided by the researcher. Pham et al. (2021c) showed that the best results can be obtained with the use of values between 1 and 10 of the parameter k.

5. Results

Initially, a gravity model was generated to estimate the applicability of the total horizontal gradient method and its enhanced versions.

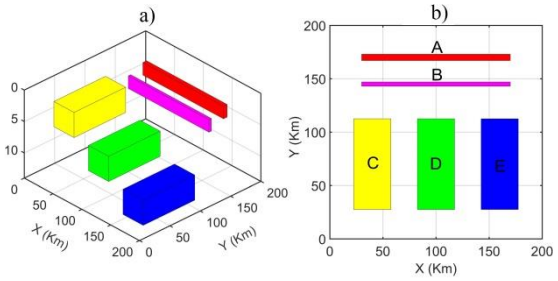

Figure 3. 3D and ground views of the model

Fig. 3a and b display the 3D and plan views of the model. Fig. 4a displays the gravity anomalies of the model. Fig. 4b displays the THG of the anomaly data in Fig. 4a. It is observed from this figure that the THG method brings clear images for the edges for the sources A and C, but responses from the bodies B, D, and E are blurred. Figure 4c displays the THGVD of the anomaly data in Fig. 4a. Although the THGVD technique produced sharper responses over the source boundaries, the obtained images for sources B, C, D, and E are fairly faint. In addition, this technique generates false boundaries around the sources A and C. Fig. 4d displays the result of the application of the BTHG detector to the anomaly data in Fig. 4a. We can see that the BTHG yielded more effective results than THG and THGVD methods in outlining all source boundaries since they can equalize the anomalies from shallow and deep bodies by using the ratio of the gradients of the THG. Fig. 4d displays the edges estimated from using the EHGA method to the anomaly in Fig. 4a. It is seen that the maxima of the EHGA are located directly over the source borders, and the results are more sharp-cut responses over the source boundaries than

those from the BTHG method. Fig. 4f displays the edges determined from using the SF technique to the anomaly in Fig. 4a. Similar to the BTHG method, the SF method equalized the signals from shallow and deep bodies. However, this method provided a boundary map having a higher resolution compared to the BTHG method.

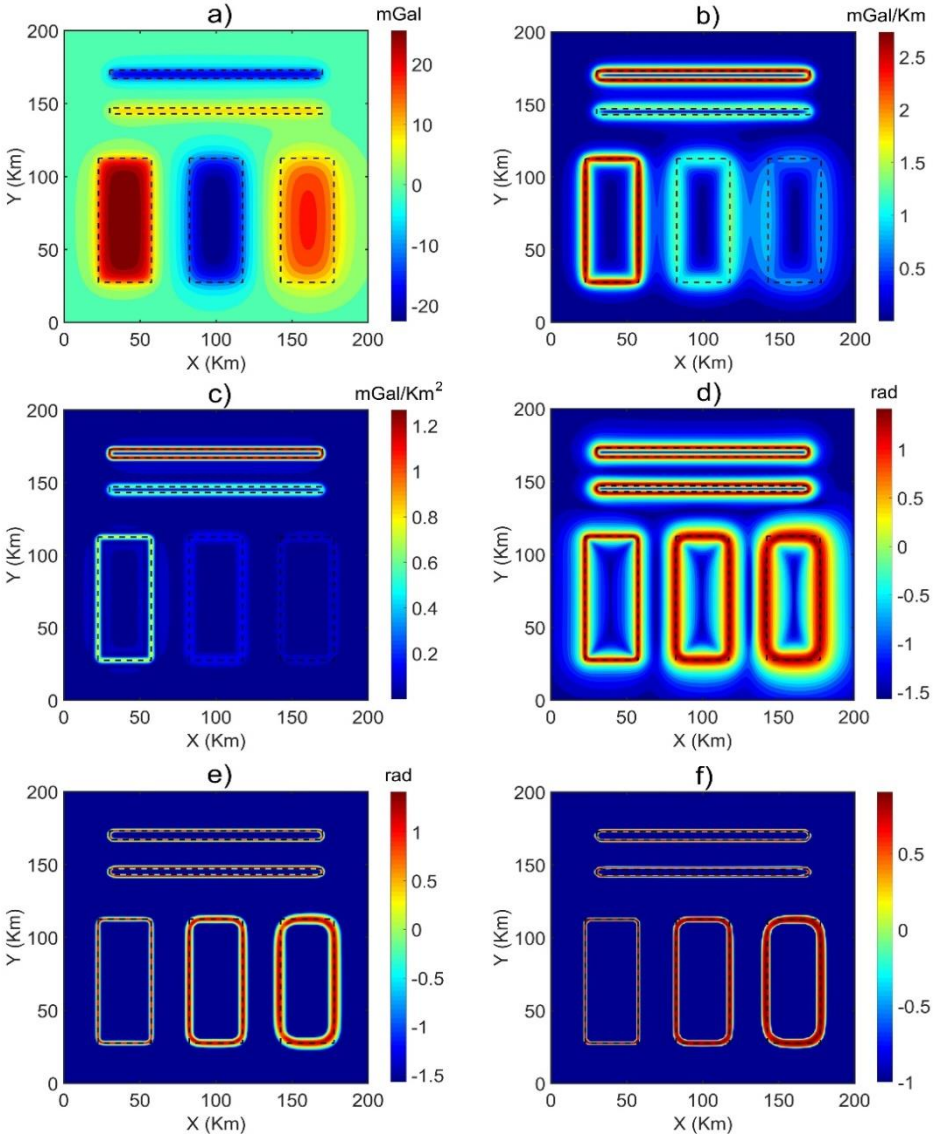

Figure 4. (a) Gravity anomaly, (b) THG, (c) THGVD, (d) BTHG, (e) EHGA, (f) SF

Since real gravity data usually contain noise, to apply techniques based on derivatives of gravity data, it is recommended to use an upward continuation filter to reduce the noise level. Fig. 5b shows the Bouguer gravity anomaly of the Hoang Sa islands after upward continuation of 2 km. Fig. 6a displays the boundaries determined by applying the THG filter to the upward-continued Bouguer gravity anomaly of the islands. In the THG filter result, it is seen that the boundaries of the more significant amplitude anomalies

prevailing in the eastern part of the area are prominent. Still, the boundaries of the lower amplitude anomalies cannot be determined (Fig. 6a). Fig. 6b displays the result obtained by application of the THGVD detector to the upward-continued Bouguer gravity anomaly. The presence of many parallel lineaments in the THGVD map is not verified by the results of the THG and the other applied methods. Thus, these have been interpreted as false boundaries around real structures, as shown in the synthetic model. Moreover, the THGVD method cannot balance gravity anomalies with different amplitudes, making it less effective in determining the borders of the deep structures. Figs. 6c, d, and e show the edges outlined by applying the BTHG, EHGA, and SF methods to the upward-continued Bouguer gravity data, respectively. As shown in the model example, the peaks of the BTHG, EHGA, and SF functions are located directly over the boundaries of geological structures. It is seen from Fig. 6c, 6d, and 6e that a large number of boundaries are delineated by these methods. Both three methods emphasize shallow and deep surface features with different wavelengths.

To estimate the depths of the gravity lineaments, we applied the curvature algorithm (Phillips et al., 2007) to the gravity in Fig. 5b (readers are referred to that paper for detailed description of the algorithm). Fig. 6f shows the result of the curvature analysis using the local wavenumber function. Fig. 7 shows the histogram of the depth estimates. We can see that most of the lineaments are found to be located in the depth range of 3 km to 9 km.

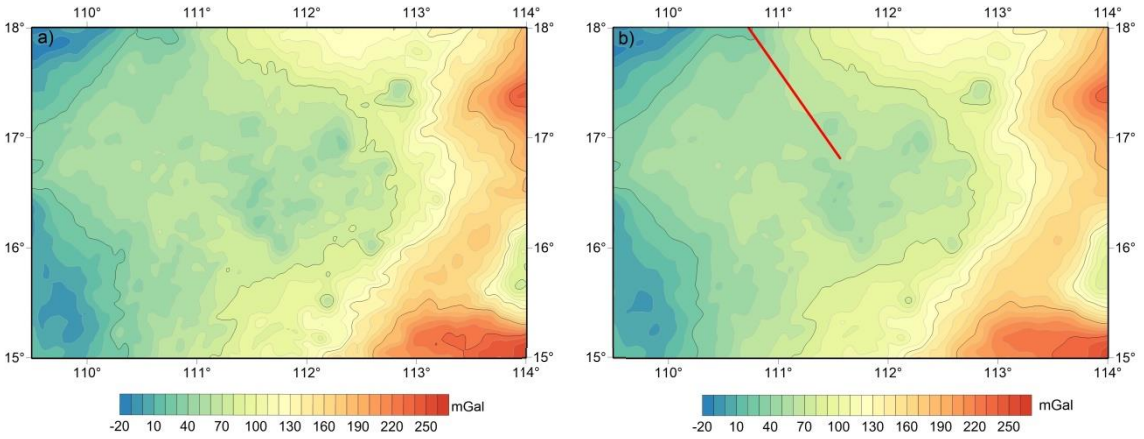

Figure 5. (a) Bouguer gravity data of the Hoang Sa islands area.
(b) Bouguer gravity data of the Hoang Sa islands area after upward continuation of 2 km.
The red line shows the seismic section in Fig. 8c, reported by Yang et al. (2018)

6. Discussions

It is clearly seen from Fig. 6a and 6b that the THG and THGVD emphasize shallow geological features with relatively short wavelengths. The reason is that these techniques use the derivative amplitudes of Bouguer gravity anomaly. The BTHG, EHGA and SF techniques are based on the ratio of the derivative amplitudes of data, therefore they can emphasize both short and long wavelengths. In other words, the BTHG, EHGA and SF methods are effective in balancing gravity anomalies with different amplitudes, and they provide clearer geological features compared to the THG and THGVD. However, it can be noted that the EHGA and SF methods provided more sharp-cut responses over the horizontal boundaries of geological structures compared to the

BTHG and other methods. For a comparison, Fig. 8 displays the interpretation results of the upward-continued gravity anomaly (Fig. 8a) along the cross-section in Fig. 5b using the EHGA and SF methods (Fig. 8b), and the interpretation result of the seismic data (Fig. 8c) reported by Yang et al. (2018). It can be seen from this figure that there is a good correlation between the boundaries determined from gravity data and seismic data with many of density boundaries indicating the faults, especially for two main faults in Fig. 8c.

Since the EHGA and SF methods produced clearer images than those from the other methods, we used these methods to highlight the lineaments of the Hoang Sa islands. Fig. 9 shows the gravity lineaments extracted from the gravity EHGA and SF maps (Figs. 6d, e). Here, the gravity lineaments were superimposed on the depth solutions (Fig. 9). A great advantage of the curvature method is that it does not depend on the window size and structure index, and does not require density information. The obtained depths show that most of the structures found in the central area are shallower than those of adjacent areas. This is in agreement with the basement structure obtained by Braitenberg et al. (2006) from inverting gravity data. Our results are also in agreement with the depth to basement from the crustal structure model of Franke et al. (2014) that showed a basement relief in 2-6 km range depth in the Hoang Sa uplift. By comparing the results in Fig. 9, we can see that many gravity lineaments match well with horizontal locations of the solutions obtained from the curvature method. However, some structures inferred by the enhancement filters in northeastern and southeastern parts of the area are not identified by the curvature algorithm (Fig. 9). This result illustrates the usefulness of the EHGA and SF filters for interpreting gravity data. In addition, it is also noteworthy that the curvature algorithm generates some new boundaries that are not extracted by the EHGA and SF filters. However, these boundaries may be spurious information that does not respond to any density structures, as pointed out by Pham et al. (2021f, g).

Fig. 10 shows the gravity lineaments superimposed on the tectonic map. As can be seen from this figure, most of the determined gravity lineaments the Hoang Sa islands are trending in the WSW-ENE, NE-SW, E-W, WNW-ESE and NNW-SSE directions. The presence of some gravity lineaments in the eastern portion of the islands (Fig. 10) is verified by the signals of the THG (Fig. 6a). The major structural features in the Hoang Sa islands area are oriented in the WSW-ENE, NE-SW and WNW-ESE directions. Some NE-SW trending boundaries compare favorably with the fault in northeastern region (Fig. 10). In addition, the peaks of the EHGA and SF filters also present a good correlation with the fault in northeastern part, which seem to be related with the boundary of the basin (Fig. 10). Note that faults in the area not always detected by the edge filters, as rocks with similar densities may be juxtaposed along a fault. Moreover, in this case, the enhancement techniques also cannot outline the boundaries of the Hoang Sa uplift. The reason could be that there is not significant difference between densities of rocks in the Hoang Sa uplift and adjacent areas as shown by the P-wave velocity model of Guo et al. (2016). The NE-SW trending boundaries in interpreted map (Fig. 10) may relate to the Shenhu tectonic movement in the northern continental margin of the Southern China by the collision of the Indian-Eurasian plate (Li et al., 2020). A series of NE-SW trending folds and belts were formed in the area by this tectonic movement (Li et al., 2020). It is obvious that the enhancement techniques are effective in extracting a wide range of density boundaries in the Hoang Sa islands. This result provides some references for further studies within geological aims in the study area.

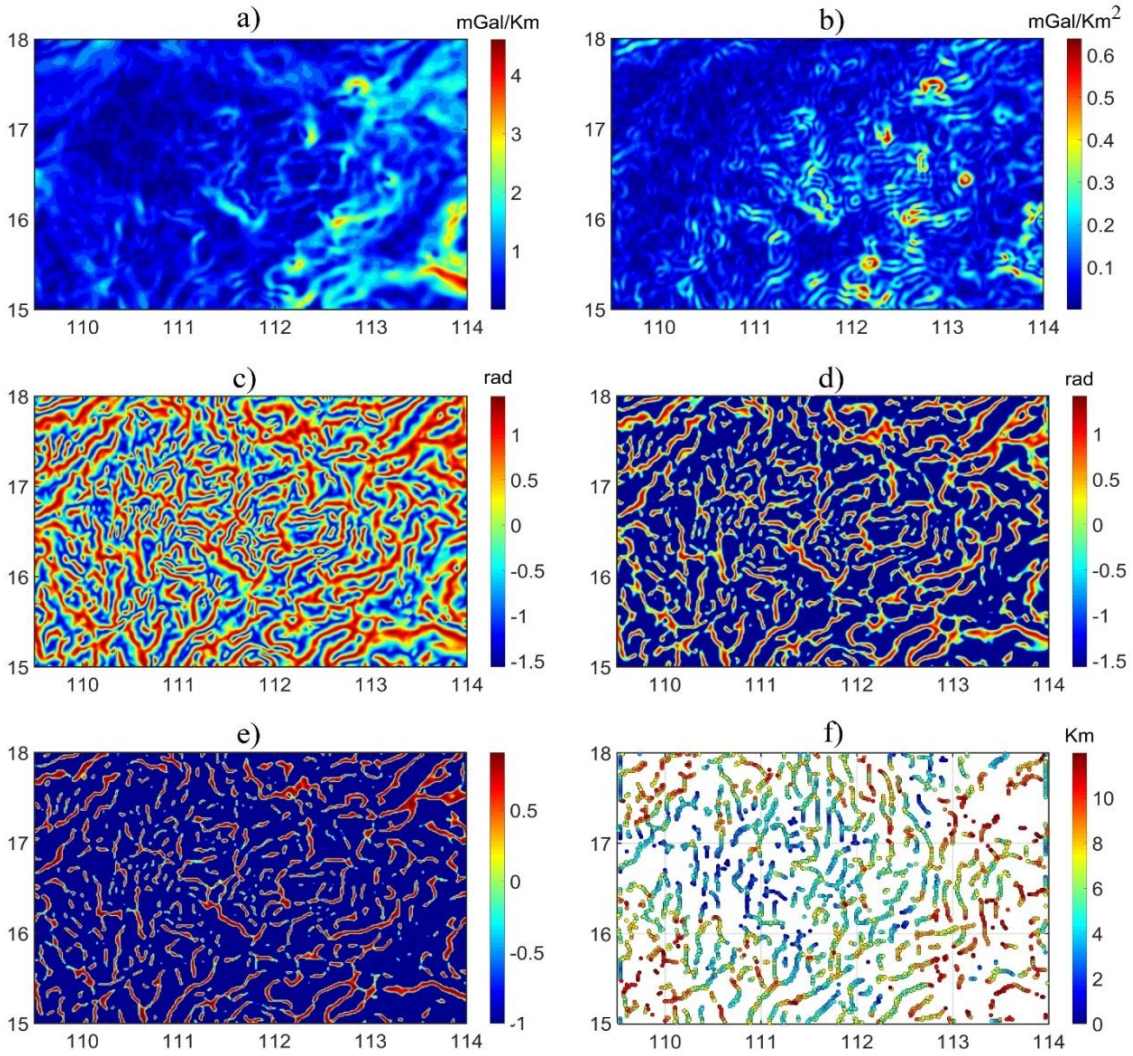

Figure 6. (a) THG, (b) THGVD, (c) BTHG, (d) EHGA, (e) SF, (f) depth solutions

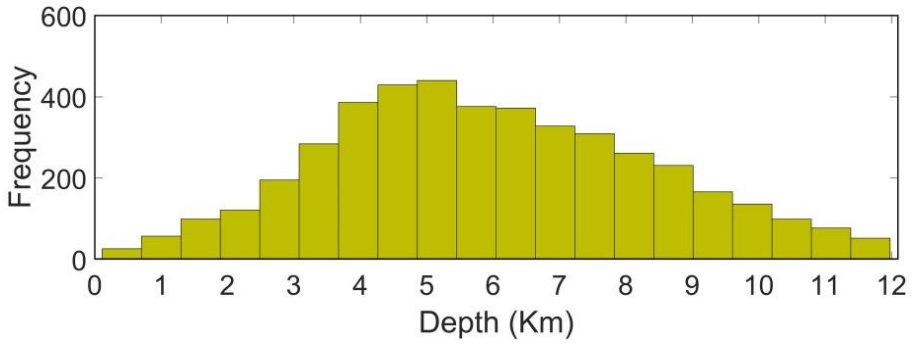

Figure 7. Histogram of the depth estimates

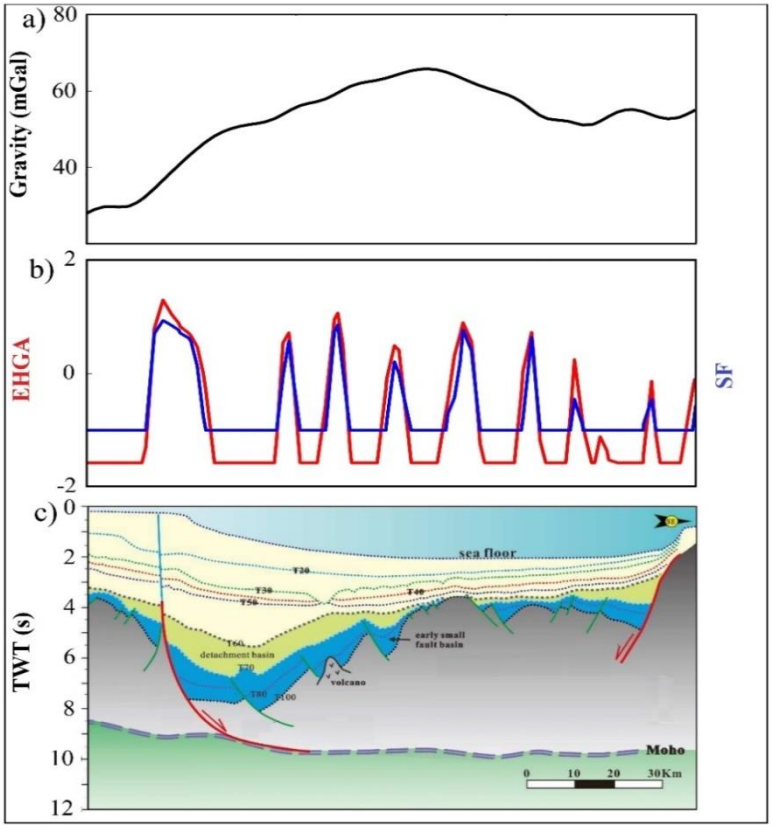

Figure 8. (a) Bouguer anomaly after upward continuation of 2 km, (b) EHGA and SF of the anomaly, (c) interpreted seismic section

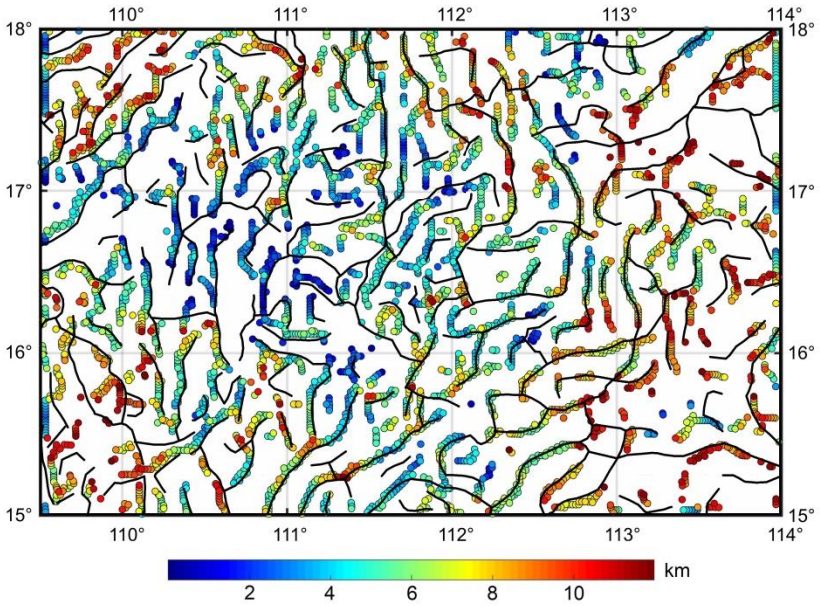

Figure 9. Gravity lineaments are superimposed on the depth estimates

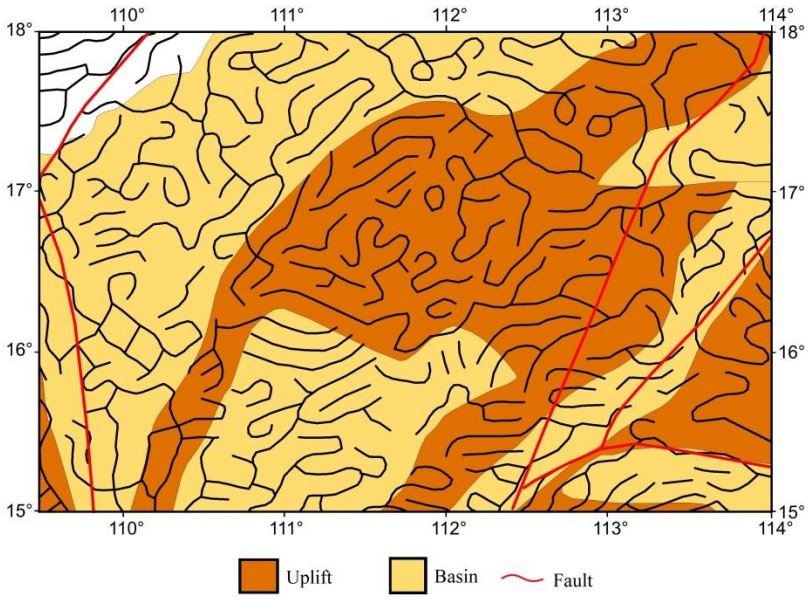

Figure 10. Gravity lineaments are superimposed on tectonic map

7. Conclusions

This study used the enhanced total horizontal gradient methods such as the THGVD, BTHG, EHGA and SF to interpret Bouguer gravity anomaly of the Hoang Sa islands. The methods were examined on synthetic data before applying them to real gravity data of the study area. The findings show that the EHGA and SF methods can give more accurate and cleaner images for the borders of the geological structures. The results determined from the interpretation of real dataset show that most of the determined structural features in the Hoang Sa islands are oriented in the WSW-ENE, NE-SW, E-W, WNW-ESE and NNW-SSE directions. The findings also show that most of the lineaments are found to be located in the depth range of 3 to 9 km. These results may contribute to future studies to better understand the geological structures of the islands.

Acknowledgements

This research has been done under the research project QG21.24 of Vietnam National University, Hanoi. Luan Thanh Pham was funded by Vingroup JSC and supported by the Postdoctoral Scholarship Programme of Vingroup Innovation Foundation (VINIF), Vingroup Big Data Institute (VinBigdata), code VINIF.2021.STS.06. The authors would like to thank three reviewers for providing valuable comments and suggestions that improved the initial version of the manuscript.

References

Bai Y., Williams S.E., Müller R.D, Liu Z., Hosseinpour M., 2014. Mapping crustal thickness using marine gravity data: Methods and uncertainties. Geophysics, 79(2), G27-G36.

Beiki M., 2010. Analytic signals of gravity gradient tensor and their application to estimate source location. Geophysics, 75(6), 159-174.

Braitenberg C., Wienecke S., Wang Y., 2006. Basement structures from satellite-derived gravity field: East Vietnam Sea ridge. Journal of Geophysical Research, 111(B5), B05407.

Briais A., Patriat P., Tapponnier P., 1993. Updated interpretation of magnetic anomalies and seafloor spreading stages in the East Vietnam Sea: implications for the tertiary tectonics of Southeast Asia. J. Geophys. Res., 98 (B4), 6299e6328.

Cooper G.R.J., Cowan D.R., 2006. Enhancing potential field data using filters based on the local phase. Computers & Geosciences, 32, 1585-1591.

Cooper G.R.J., Cowan D.R., 2008. Edge enhancement of potential-field data using normalized statistics. Geophysics, 73, H1-H4.

Cordell L., Grauch V.J.S., 1985. Mapping basement magnetization zones from aeromagnetic data in the San Juan basin New Mexico. The utility of regional gravity and magnetic anomaly maps. Doi: 10.1190/1.0931830346.ch16.

Dung N.K., Thanh D.D., Vuong H.V., Cuong, D.H., Dung T.T., Dai N.B., Duong T.T., 2019. A detailed research on the structural characteristics of Hoang Sa and Truong Sa archipelagos - East Vietnam Sea based on gravity data analysis. Vietnam Journal of Marine Science and Technology, 19(3B), 163-175 (in Vietnamese).

Dung T.T., Kulinich R.G., Sang N.V., Que B.C., Dai N.B., Dung N.K., Dung T.T., Lap T.T., 2019. Improving accuracy of altimeter-derived marine gravity anomalies for geological structure research in the Vietnam South-Central continental shelf and adjacent areas. Russ. J. Pac. Geol., 13(4), 364-374.

Dung T.T., Que B.C., Phuong N.H., 2013. Cenozoic basement structure of the East Vietnam Sea and adjacent areas by modeling and interpreting gravity data. Russian Journal of Pacific Geology, 7(4), 227-236.

Echogdali F.Z., Boutaleb S., Abia E.H., Ouchchen M., Dadi B., Id-Belqas M., Abioui M., Pham L.T., Abu-Alam T., Mickus K.L., 2021. Mineral prospectivity mapping: a potential technique for sustainable mineral exploration and mining activities - a case study using the copper deposits of the Tagmout basin, Morocco. Geocarto International, 1-22. Doi: 10.1080/10106049.2021.2017006.

Eldosouky A.M., El-Qassas R.A.Y., Pham L.T., Abdelrahman K., Alhumimidi M.S., El Bahrawy A., Mickus K., Sehsah H., 2022a. Mapping Main Structures and Related Mineralization of the Arabian Shield (Saudi Arabia) Using Sharp Edge Detector of Transformed Gravity Data. Minerals, 12, 71.

Eldosouky A.M., Pham L.T., Abdelrahman K., Fnais M.S., Gomez-Ortiz D., 2022b. Mapping structural features of the Wadi Umm Dulfah area using aeromagnetic data. Journal of King Saud University - Science, 34(2), 101803.

Eldosouky A.M., Pham L.T., El-Qassas R.A.Y., Hamimi Z., Oksum E., 2021a. Lithospheric Structure of the Arabian-Nubian Shield Using Satellite Potential Field Data. In: Hamimi Z., Fowler AR., Liégeois JP., Collins A., Abdelsalam M.G., Abd EI-Wahed M. (eds) The Geology of the Arabian-Nubian Shield. Regional Geology Reviews. Springer, Cham.

Eldosouky A.M., Pham L.T., Henaish A., 2022c. High precision structural mapping using edge filters of potential field and remote sensing data: A case study from Wadi Umm Ghalqa area, South Eastern Desert, Egypt. The Egyptian Journal of Remote Sensing and Space Science. Doi: 10.1016/j.ejrs.2022.03.001.

Eldosouky A.M., Pham L.T., Mohmed H., Pradhan B., 2020. A comparative study of THG, AS, TA, Theta, TDX and LTHG techniques for improving source boundaries detection of magnetic data using synthetic models: a case study from G. Um Monqul, North Eastern Desert, Egypt. J. Afr. Earth Sci., 170, 103940.

Eldosouky A.M., Pour A.B., Hamed A., Taha A., Gamal M., Mahmoud A., Pham L.T., 2021b. Utilization of Landsat-8 Imagery and Aeromagnetic Data for Deciphering Alteration Zones and Structures: Implications for Mineral Exploration in the Southeastern Desert of Egypt, Frontiers in Scientific Research and Technology, 2, 19-28.

Fedi M., Florio G., 2001. Detection of potential fields source boundaries by enhanced horizontal derivative method. Geophys Prospect., 49, 40-58.

Ferreira F.J.F., de SouzaJ., de Bongiolo A.B.e.S., de Castro L.G., 2013. Enhancement of the total horizontal gradient of magnetic anomalies using the tilt angle. Geophysics, 78(3), J33-J41.

Franke D., Savva D., Pubellier M., Steuer S., Mouly B., Auxietre J.L., Meresse F., Chamot-Rooke N., 2014. The final rifting evolution in the East Vietnam Sea. Marine and Petroleum Geology, 58, 704-720.

Ghomsi F.E.K., Pham L.T., Tenzer R., Esteban F.D., Vu T.V., Kamguia J., 2022b. Mapping of fracture zones and structural lineaments of the Gulf of Guinea passive margins using marine gravity data from CryoSat-2 and Jason-1 satellites. Geocarto International, 1-24.
Doi: 10.1080/10106049.2022.2040602.

Ghomsi F.E.K., Ribeiro-Filho N., Baldez R., Tenzer R., Martins C.M., Chisenga C., Nguiya S., Nouayou R., 2022a. Identification of Cameroon's geological structures through a gravity separation and using seismic crustal models. J. Afr. Earth Sci., 173, 104027.

Guo X.R., Zhao M.H., Huang H.B., Qiu X.L., Wang J., He E.Y., Zhang J.Z., 2016. Crustal structure of Xisha block and its tectonic attributes. Chinese Journal of Geophysics, 59(3), 288-300.

Hsu S.K., Coppense D., Shyu C.T., 1996. High-resolution detection of geologic boundaries from potential field anomalies: An enhanced analytic signal technique. Geophysics, 61, 1947-1957.

Kafadar O., 2017. CURVGRAV-GUI: a graphical user interface to interpret gravity data using curvature technique. Earth Science Informatics, 10(4), 525-537.

Kafadar O., 2022. Applications of the Kuwahara and Gaussian filters on potential field data. Journal of Applied Geophysics, 198, 104583.

Kha T.V., Trung N.N., 2020. A novel method for computing the vertical gradients of the potential feld: application to downward continuation. Geophys. J. Int., 220(2), 1316-1329.

Kha V.T., Vuong V.H., Thanh D.D., Hung Q.D., Anh D.L., 2018. Improving a maximum horizontal gradient algorithm to determine geological body boundaries and fault systems based on gravity data. Journal of Applied Geophysics, 152, 161-166.

Li F., Sun Z., Pang X., Liao J., Yang H., Xie H., Zhuo H., Zhao Z., 2019. Low-viscosity crustal layer controls the crustal architecture and thermal distribution at hyperextended margins: Modeling insight and application to the northern East Vietnam Sea margin. Geochemistry, Geophysics, Geosystems, 20.

Li W., Li J., Wang X., 2020. Deep crustal structure imaging of gravity and magnetic anomalies in the Xisha Trough, China. Arabian Journal of Geosciences, 13(1), 32.

Liem N.V., Trinh P.T., Phong T.V., Lien V.T.H., Huong N.V., Xuyen N.Q., Thanh B.N., Hao D.V., Pham B.T., Dung N.V., Dang V.K., An V.H., 2021. Pliocene - present tectonics and strain rate in Ninh Thuan region and surrounding continental shelf. Vietnam J. Earth Sci., 43(1), 33-56.

Long H.V., Thanh N.T., Tuan V.T., Tung N.T., Anh N.L., Din D.B., Duc L.V., Dien T.N., Hiep N.H., 2021. Holocene sedimentation offshore Southeast Vietnam based on geophysical interpretation and sediment composition analysis. Vietnam J. Earth Sci., 43(3), 336-379.

Lu Y., Li W., Wu S., Cronin B.T., Lu F., Wang B., Yang T., Ma B., 2018. Morphology, architecture, and evolutionary processes of the Zhongjian Canyon between two carbonate platforms, East Vietnam Sea. Interpretation, 6(4), SO1-SO15.

Luong L.D., Hoang N., Shinjo R., B. Shakirov R., Obzhirov A., 2021. Chemical, mineralogical, and physicochemical features of surface saline muds from Southwestern sub-basin of the East Vietnam Sea: Implication for new peloids. Vietnam J. Earth Sci., 43(4), 496-508.

Melouah O., Pham L.T., 2021. Improved ILTHG method for edge enhancement of geological structures: application to gravity data from the Oued Righ valley. J. Afr. Earth Sci., 177, 104162.

Miller H.G., Singh V., 1994. Potential field tilt a new concept for location of potential field sources. J. Appl. Geophys., 32(2-3), 213-217.

Nasuti Y., Nasuti A., Moghadas D., 2019. STDR: a novel approach for enhancing and edge detection of potential field data. Pure Appl Geophys., 176(2), 827-841.

Oksum E., Dolmaz M.N., Demir M., Pham L.T., 2021a. Evaluation of magnetic data of an emery bearing ore field by edge detection methods: Muğla, Türkiye example. Journal of Engineering Sciences and Design, 9(1), 319-329 (in Turkish).

Oksum E., Dolmaz M.N., Pham L.T., 2019. Inverting gravity anomalies over the Burdur sedimentary basin, SW Turkey. Acta Geod. Geophys., 54, 445-460.

Oksum E., Le D.V., Vu M.D., Nguyen T.H.T., Pham L.T., 2021b. A novel approach based on the fast sigmoid function for interpretation of potential field data. Bulletin of Geophysics and Oceanography, 62(3), 543-556.

Pham L.T., 2020. A comparative study on different filters for enhancing potential field source boundaries: synthetic examples and a case study from the Song Hong Trough (Vietnam). Arab J. Geosci., 13(15), 723.

Pham L.T., 2021. A high-resolution edge detector for interpreting potential field data: a case study from the Witwatersrand basin, South Africa. J. Afr. Earth Sci., 178, 104190.

Pham L.T., Do T.D., Oksum E., 2018b. A new method for edge detection in interpretation of potential feld data. Journal of Engineering Sciences and Design, 6(4), 637-642.

Pham L.T., Eldosouky A.M., Oksum E., Saada S.A., 2020a. A new high resolution filter for source edge detection of potential field data. Geocarto International, 1-18.
Doi: 10.1080/10106049.2020.1849414.

Pham L.T., Kafadar O., Oksum E., Hoang-Minh T., 2021g. A comparative study on the peak detection methods used to interpret potential field data: a case study from Vietnam. Geocarto International, 1-18. Doi: 10.1080/10106049.2021.2007297.

Pham L.T., Nguyen D.A., Eldosouky A.M., Abdelrahman K., Vu T.V., Al-Otaibi N., Ibrahim E., Kharbis S., 2021d. Subsurface structural mapping from high-resolution gravity data using advanced processing methods. J. King Saud Univ. Sci., 33(5), 101488.

Pham L.T., Oksum E., Le D.V., Ferreira F.J.F., Le S.T., 2021c. Edge detection of potential field sources using the softsign function. Geocarto International, 1-14. Doi: 10.1080/10106049.2021.1882007.

Pham L.T., Oksum E., Nguyen D.V., Eldosouky A.M., 2021a. On the performance of phase-based filters for enhancing lateral boundaries of magnetic and gravity sources: a case study of the Seattle Uplift. Arab J. Geosci., 14, 129.

Pham L.T., Oksum E., Vu M.D., Vo Q.T., Le-Viet K.D., Eldosouky A.M., 2021f. An improved approach for detecting ridge locations to interpret the potential field data for more accurate structural mapping: a case study from Vredefort dome area (South Africa). J. Afr Earth Sci., 175, 104099.

Pham L.T., Oliveira S.P., Le M.H., Trinh P.T., Vu T.V., Duong V.H., Ngo T.N.T., Do T.D., Nguyen T.H., Eldosouky A.M., 2021e. Delineation of structural lineaments of the Southwest Sub-basin (East Vietnam Sea) using global marine gravity model from CryoSat-2 and Jason-1 satellites. Geocarto International, 1-18.
Doi: 10.1080/10106049.2021.1981463.

Pham L.T., Vu M.D., Le S.T., 2021b. Performance Evaluation of Amplitude- and Phase Based Methods for Estimating Edges of Potential Field Sources. Iran J. Sci. Technol. Trans. Sci., 45, 1327-1339.

Pham L.T., Vu T.V., Le-Thi S., Trinh P.T., 2020b. Enhancement of potential field source boundaries using an improved logistic filter. Pure Appl. Geophys., 177, 5237-5249.

Phillips J.D., Hansen R.O., Blakely R.J., 2007. The use of curvature in potential-field interpretation. Explor Geophys., 38(2), 111-119.

Prasad K.N.D., Pham L.T., Singh A.P., 2022. Structural mapping of potential field sources using BHG filter. Geocarto International, 1-28.
Doi: 10.1080/10106049.2022.2048903.

Roest W.R., Verhoef J., Pilkington M., 1992. Magnetic interpretation using the 3-D analytic signal. Geophysics, 57, 116-125.

Saibi H., Nishijima J., Hirano T., Fujimitsu Y., Ehara S., 2008. Relation between structure and lowtemperature geothermal systems in Fukuoka city, southwestern Japan. Earth Planets Space., 60(8), 821-826.

Sandwell D.T., Muller R.D., Smith W.H.F., Garcia E., Francis R., 2014. New global marine gravity model from CryoSat-2 and Jason-1 reveals buried tectonic structure. Science, 346(6205), 65-67.

Smith W.H.F., Sandwell D.T., 1997. Global seafloor topography from satellite altimetry and ship depth soundings. Science, 277(5334), 1956-1962.

Tang H., Guo T, Wu K., Liu Z., Xu J., Lu B., Wang P., 2022. Reassessment of the Distribution of Mantle CO_2 in the Bohai Sea, China: The Perspective from the Source and Pathway System. Acta. Geologica Sinica, 96(1), 337-347.

Tapponnier P., Peltzer G., Armijo R., 1986. On the mechanics of the collision between India and Asia, in Collision Tectonics, edited by M.P. Coward and A. C. Ries, Geol. Soc. Spec. Publ., 19, 115-157.

Tatchum C.N., Tabod T.C., Koumetio F., Manguelle-Dicoum E., 2011. A Gravity Model Study for Differentiating Vertical and Dipping Geological Contacts with Application to a Bouguer Gravity Anomali Over the Foumban Shear Zone, Cameroon. Geophysica, 47(1-2), 43-55.

Taylor B., Hayes D.E., 1983. Origin and history of the East Vietnam Sea basin. In: Hayes, D.E. (Ed.), The Tectonic and Geologic Evolution of Southeast Asian

Seas and Islands; Part 2. Geophysical Monograph, 23-56.

Trung N.N., Hong P.T., Nam B.V., Huong N.T.T., Lap T.T., 2018. Moho depth of the northern Vietnam and Gulf of Tonkin from 3D inverse interpretation of gravity anomaly data, J. Geophys. Eng., 15, 1651-1662.

Trung N.N., Huong N.T.T., 2013. Topography of the Moho and earth crust structure beneath the East Vietnam Sea from 3D inversion of gravity field data. Acta Geophys., 61(2), 357-384.

Trung N.N., Kha T.V., Nam B.V., Huong N.T.T., 2020. Sedimentary basement structure of the Southwest Sub-basin of the East Vietnam Sea by 3D direct gravity inversion. Mar Geophys Res., 41(1), 7.

Verduzco B., Fairhead J.D., Green C.M., MacKenzie C., 2004. New insights into magnetic derivatives for structural mapping. The Leading Edge, 23, 116-119.

Wijns C., Perez C., Kowalczyk P., 2005. Theta map: Edge detection in magnetic data. Geophysics, 70, 39-43.

Wu F., et al., 2021. Early development of carbonate platform (Xisha Islands) in the northern East Vietnam Sea. Marine Geology, 441, 106629.

Xu J., Ben-Avraham Z., Kelty T., Yu H.S., 2014. Origin of marginal basins of the NW Pacific and their plate tectonic reconstructions. Earth-Science Reviews, 130, 154-196.

Yang L., Ren J., McIntosh K., Pang X., Chao L., Zhao Y., 2018. The structure and evolution of deepwater basins in the distal margin of the northern East Vietnam Sea and their implications for the formation of the continental margin. Marine and Petroleum Geology, 92, 234-254.

Yu C., Xu M., Kirby J.F., Shi X., Jimenez-Diaz A., 2022. Spatial variations of the effective elastic thickness and internal load fraction in the Cascadia subduction zone. Geophys. J. Int., 229, 487-504.